A direct measurement of rotatable and frozen CoO spins in exchange bias system of CoO/Fe/Ag(001)

J. Wu[1], J. S. Park,[1] W. Kim[1, 2], E. Arenholz,[3] M. Liberati,[3] A. Scholl,[3] Y. Z. Wu,[4] Chanyong Hwang[2], and Z. Q. Qiu[1]

[1] Department of Physics, University of California at Berkeley, Berkeley, California 94720, USA

[2] Korea Research Institute of Standards and Science,Yuseong, Daejeon 305-340, Koera

[3] Advanced Light Source, Lawrence Berkeley National Laboratory, Berkeley, California 94720, USA

[4] Dept. of Physics, Fudan University, Shanghai, P. R. China

Abstract

The exchange bias of epitaxially grown CoO/Fe/Ag(001) was investigated using X-ray Magnetic Circular Dichroism (XMCD) and X-ray Magnetic Linear Dichroism (XMLD) techniques. A direct XMLD measurement on the CoO layer during the Fe magnetization reversal shows that the CoO compensated spins are rotatable at thinner thickness and frozen at larger thickness. By a quantitative determination of the rotatable and frozen CoO spins as a function of the CoO film thickness, we find the remarkable result that the exchange bias is well established before frozen spins are detectable in the CoO film. We further show that the rotatable and frozen CoO spins are uniformly distributed in the CoO film.

PACS numbers: 75.70.Ak

As a ferromagnetic(FM)/antiferromagnetic(AFM) system is cooled down within a magnetic field to below the Néel temperature (T_N) of the AFM material, the shift of the FM hysteresis loop in the magnetic field is referred to as exchange bias [1]. Investigation of exchange bias has been one of the most active research areas because of its importance to spintronics technology [2]. While it is well accepted that the AFM order is responsible for the exchange bias [3,4], it remains a mystery on how the AFM spins behave during the FM magnetization reversal. Consequently, different AFM spin structures have been proposed to explain the exchange bias [5,6,7,8]. Most measurements are based on the FM layer hysteresis loops which explore only indirectly the AFM spin behavior [9,10,11,12,13,14,15,16,17]. Recently, the development of X-ray Magnetic Circular Dichroism (XMCD) and X-ray Magnetic Linear Dichroism (XMLD) [18] allows an element-specific study of the FM/AFM systems. The result shows clearly a correlation between the FM and the AFM domains, and the existence of a small amount of uncompensated spins in the AFM layer [19]. It was further shown that only a small percentage of the uncompensated spins is pinned to account for the exchange bias [20,21,22,23] and that these pinned uncompensated AFM spins actually extend into the AFM layer [24], suggesting a bulk-like effect of the AFM spins in the exchange bias [25,26,27,28,29]. Despite the above progress, the compensated AFM spin behavior remains unclear during the FM layer reversal. It is usually assumed that the AFM compensated spins should be frozen to generate an exchange bias. However, one direct measurement on Co/bulk NiO(001) shows that the NiO spins at the Co/NiO interface may exhibit a spring-like winding structure during the Co magnetization alignment [30]. This result raises a critical issue, i.e. whether it is necessary to freeze the majority of the AFM compensated spins to generate an exchange bias in a FM/AFM thin film system. In this Letter, we report an experimental study of CoO/Fe/Ag(001) single crystalline thin films. We find the remarkable result that as the CoO thickness increases, the exchange bias is well established before frozen spins are detectable in CoO film.

A Ag(001) substrate was prepared in an ultra-high vacuum system by cycles of Ar ion sputtering at ~2keV and annealing at 600^{o}C. A 15 monolayer (ML) Fe film was grown on top of the Ag(001) substrate. Then a CoO wedge (0-8 nm) was grown on top of the Fe film by a reactive deposition of Co under an oxygen pressure of 1×10^{-6} Torr. Low Energy Electron Diffraction (LEED) shows well-defined diffraction spots, indicating the formation of single crystalline CoO film [31]. The sample is covered by a 2nm Ag

protection layer and then measured at beamlines 4.0.2 and 11.0.1 of the Advanced Light Source (ALS). Fe film on Ag(001) has a bcc structure with the Fe [001] axis parallel to the Ag [110] axis and CoO film on Fe(001) has an fcc structure with the CoO [110] axis parallel to the Fe [100] axis.

XMLD effect is clearly seen by measuring the X-ray absorption spectrum (XAS) at the CoO L_3 edge (Fig. 1) at the normal incidence. The L_3 ratio (R_{L3}), defined as the ratio of the XAS intensity at 778.1 eV and at 778.9 eV, is used to quantify the XMLD effect [32]. The sample of CoO(6 nm)/Fe(15 ML)/Ag(001) was cooled to 90 K and measured by PEEM-3 with the incident x-ray at 60^o incident angle and circularly polarized for Fe domain imaging, and linearly polarized for CoO domain imaging. The CoO domains follow exactly the Fe domains (Fig. 1b). Noting that Fe [100] axis is parallel to CoO [110] axis, then based on the L_3 line shape and ratio analysis [32,33,34,35], we conclude that the in-plane CoO AFM spins have a 90^o-coupling to the Fe spins in the CoO(6 nm)/Fe(15ML)/Ag(001) sample.

After the sample was cooled down to 90 K within a 4 kOe magnetic field along the Fe [100] crystal axis, Fe and CoO hysteresis loops are measured at 90 K with the applied field in the field cooling direction. A small transverse in-plane field was applied during the hysteresis loop measurement to ensure a rotational Fe magnetization reversal. In the XMLD measurement of the CoO L_3 edge, the x-ray polarization direction is also parallel to the field cooling direction. Since the exchange bias and the amount of rotatable/frozen spins could depend on the field frequency [36], we performed all our measurements in the DC regime. The most interesting observation is the appearance of the CoO XMLD hysteresis loop (Fig. 2) in d_{CoO}=2.0 nm sample, showing clearly that the CoO compensated spins rotate during the Fe magnetization reversal. In contrast, the absence of the CoO hysteresis loop in d_{CoO}=6.0 nm sample shows that the CoO spins are totally frozen during the Fe magnetization reversal.

Fig. 3 shows the Fe film coercivity (H_C) and exchange bias (H_E) as a function of the CoO thickness. While the H_C starts to increase at d_{CoO}~0.2 nm, the H_E develops only above a critical thickness of d_{CoO}=0.8 nm. The increase of the H_C is due to the establishment of the AFM order of the CoO layer [2]. Then the onset of H_E at d_{CoO}=0.8 nm shows that the exchange bias does not develop right after the CoO establishes its AFM order. We further carried out the following measurement to separate the rotatable and frozen spins in the CoO layer. We performed XMLD measurement as a function of the

polarization angle (ϕ) to obtain the ϕ-dependence of the L_3 ratio R_{L3}, $R_{L3}=A\cos^2\phi+B$, with the coefficient *A* proportional to the amount of the AFM compensated spins. Therefore a R_{L3}-ϕ measurement allows the determination of the amount of AFM spins under specific conditions.

We first measured the R_{L3}-ϕ dependence right after the field cooling. Under this condition, both rotatable and frozen CoO spins should be aligned to the same direction so that the R_{L3} difference at $\phi=90^o$ and $\phi=0^o$ [e.g., $\Delta R_{L3}=R_{L3}(90^o)-R_{L3}(0^o)$] is proportional to the total CoO spins (top row of Fig. 4). We then rotate the in-plane magnetic field by 90^o to rotate the Fe magnetization by 90^o in the film plane. Under this condition, the rotatable CoO spins should follow the Fe magnetization to rotate by 90^o while the frozen CoO spins should remain in their original direction. Then ΔR_{L3} in this case should correspond to the difference between the frozen spins and the rotatable spins inside the CoO film. The result (lower row of Fig. 4) indeed shows a thickness dependent ΔR_{L3}. At d_{CoO}=6.0 nm, the R_{L3}-ϕ dependence remains unchanged after the field rotates by 90^o, showing that there is no rotatable spins at this thickness. As the CoO thickness decreases to d_{CoO}=2.5 nm, ΔR_{L3} decreases, showing that some CoO spins rotate away from the field cooling direction in the CoO film. Thinner than d_{CoO}=2.5nm, ΔR_{L3} reverses its sign, showing that there are more rotatable spins than frozen spins in the CoO film. The difference of ΔR_{L3} for field parallel and perpendicular to the field cooling direction allows us to determine quantitatively the percentage of the frozen spins in the CoO film (Fig. 3). The CoO film has no detectable frozen spins below 2.2 nm (with an error bar of ~0.16 nm), becomes partially frozen for 2.2 nm<d_{CoO}<4.5 nm, and has all spins frozen for d_{CoO}>4.5 nm. We then find the remarkable result that the exchange bias develops even when no frozen CoO spins are detectable at d_{CoO}<2.2 nm, reaches ~2/3 of its saturation value at the onset of the frozen spins at d_{CoO}=2.2 nm, and becomes saturated at d_{CoO}=3 nm where 80% of the CoO spins are frozen. We estimate an upper limit of no more than ~5% of frozen spins below d_{CoO}=2.2 nm. Therefore we conclude that ~5% frozen CoO spins should be enough to generate an exchange bias in CoO/Fe/Ag(001) system. This result may explain why only a small percentage of pinned uncompensated spins would be enough to account for the exchange bias [20-24].

The next question is where the rotatable and frozen CoO spins are located? To answer this question, we inserted a 2 ML NiO probe layer at the CoO/Fe interface and at the surface of CoO/Fe by growing two samples of CoO(wedge)/NiO(2 ML)/Fe(15

ML)/Ag(001) and NiO(2 ML)/CoO(wedge)/Fe(15 ML)/Ag(001), and measured the Ni XMLD as a function of the CoO thickness. The result shows that the NiO XMLD follows exactly the CoO thickness dependence (Fig. 5). This result shows that the rotatable and frozen spins distribute uniformly inside the entire CoO film, supporting the doping and FM/AFM/FM results [25-29] that the exchange bias depends on the bulk AFM spin structure. It should be mentioned that the NiO spins are much softer than CoO spins due to a much weaker NiO magnetic anisotropy [37]. Consequently, the inserted 2 ML NiO won't produce a noticeable shift of CoO onset thickness for the frozen spins.

The last question is the role of FeO layer at the Fe-CoO interface. The interfacial FeO layer was identified to be only in the monolayer regime [38,39,40] and won't alter the exchange bias of Fe/CoO system [41]. In addition, the fact that we have the same FeO interface at different CoO thicknesses allows us to single out the effect of the AFM thickness on the exchange bias. We conclude that the presence of the FeO interfacial layer does *not* alter our conclusion.

In summary, we investigated epitaxially grown CoO/Fe/Ag(001). Using element-specific XMLD measurement, we find that the CoO spins are rotatable below 2.2 nm CoO thickness, become partially frozen between 2.2 nm and 4.5 nm, and totally frozen above 4.5 nm. Contrary to the expectation, the exchange bias of the Fe film develops at d_{Co}>0.8 nm even when no frozen spins are detectable in CoO film, reaches ~2/3 of its saturation value at the onset of frozen CoO spins at d_{Co}=2.2 nm, and saturates at d_{CoO}=3 nm where 80% of the CoO spins are frozen. With the XMLD sensitivity estimation, we conclude that ~5% of frozen CoO spins is enough to establish the exchange bias in CoO/Fe/Ag(001) system. We further show that the rotatable/frozen spins distribute uniformly in the CoO film.

Acknowledgement

This work was supported by National Science Foundation DMR-0803305, U.S. Department of Energy DE-AC02-05CH11231, KICOS through Global Research Laboratory project, and Chinese Education Department.

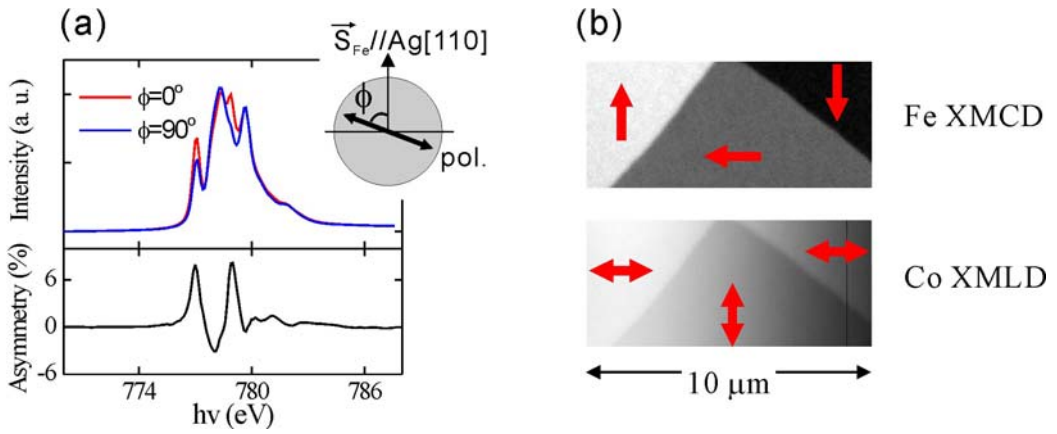

Fig. 1: (color online) (a) X-ray Absorption Spectra (XAS) of Co L_3 edge taken at two orthogonal linear polarizations ($\phi=0^o$ and 90^o) for CoO(6.0 nm)/Fe(15 ML)/Ag(001). The asymmetry of two spectra represents XMLD signal. (b) Magnetic domain images of ferromagnetic Fe and antiferromagnetic CoO taken by XMCD and XMLD, respectively. Arrows indicate the orientation of Fe and CoO spins. It is clear that the antiferromagnetic CoO spins are 90^o coupled to Fe spins.

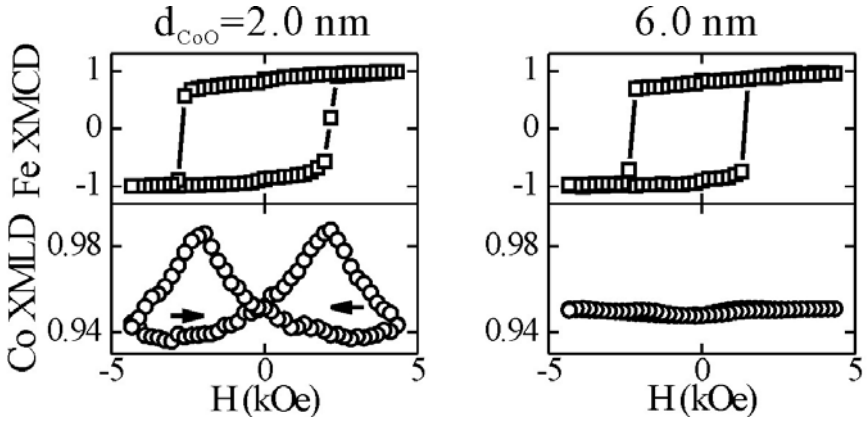

Fig. 2: Hysteresis loops of ferromagnetic Fe and antiferromagnetic CoO for CoO/Fe(15 ML)/Ag(001) taken by XMCD and XMLD, respectively. Arrows indicate the ramping direction of magnetic field. The presence and absence of the CoO response to the magnetic field at d_{CoO}=2.0 nm and at d_{CoO}=6.0 nm show rotatable and frozen compensated spins in the 2.0 nm and 6.0 nm thick CoO films respectively.

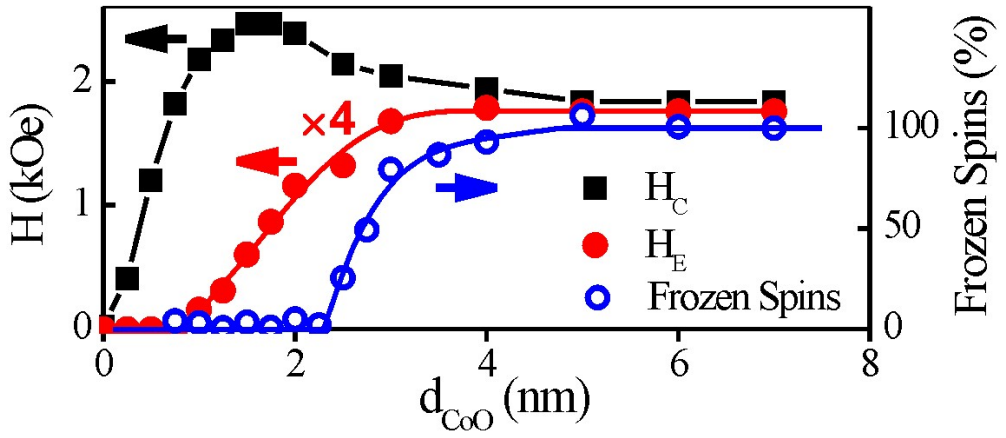

Fig. 3: (color online) Fe film coercivity (H_C), exchange bias (H_E) and the percentage of CoO frozen spins in CoO/Fe(15ML)/Ag(001) as a function of CoO thickness. The remarkable fact is that H_E develops below 2.2 nm CoO thickness where no frozen CoO spins are detectable. The solid lines are guides to eyes.

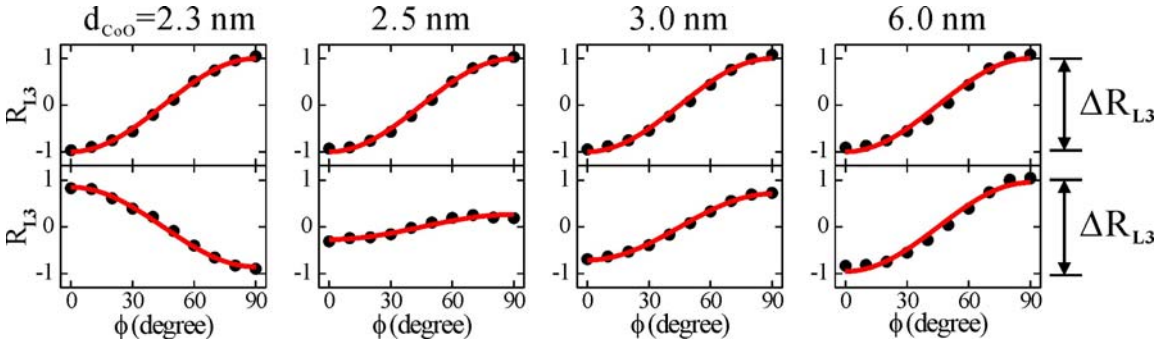

Fig. 4: (color online) Polarization angle dependence of the Co L_3 ratio measured with a 0.4 Tesla in-plane magnetic field at different CoO thicknesses in CoO/Fe(15 ML)/Ag(001). Solid lines are fitting results of $\cos^2\phi$-dependence. The L_3 ratio difference $\Delta R_{L3}=R_{L3}(90^o)-R_{L3}(0^o)$ is proportional to the sum and subtraction of the frozen and rotatable CoO spins for field parallel (top row) and perpendicular (lower row) to the field cooling direction, respectively.

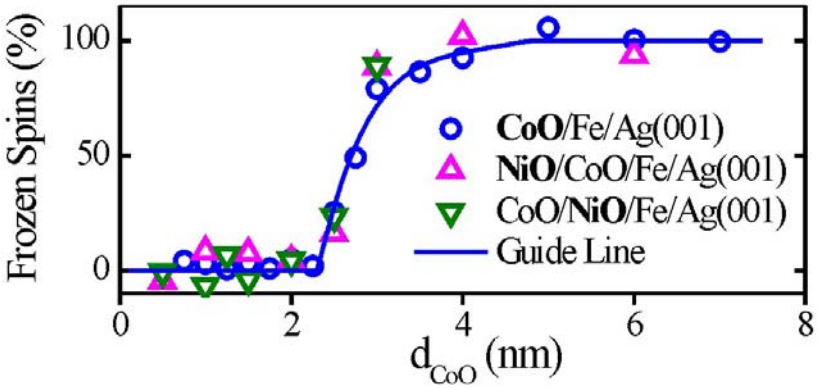

Fig. 5: (color online) A 2ML NiO layer is inserted on the top or bottom of CoO to detect the depth-dependent distribution of the frozen CoO spins. The same thickness dependences of the frozen CoO and NiO spins indicate a uniform distribution of the frozen spins in the CoO film.

References:

1. W. H. Meiklejohn and C. P. Bean, Phys. Rev. **102**, 1413 (1956).
2. J. Nogues and I. K. Schuller, J. Magn. Magn. Mater. **192**, 203 (1999).
3. M. G. Blamire, M. Ali, C.-W. Leung, C. H. Marrows, and B. J. Hickey, Phys. Rev. Lett. **98**, 217202 (2007).
4. E. Shipton, K. Chan, T. Hauet T, O. Hellwig, and E. E. Fullerton, Appl. Phys. Lett. **95**, 132509 (2009).
5. N.C. Koon, Phys. Rev. Lett. **78**, 4865 (1997).
6. T. C. Schulthess and W. H. Butler, Phys. Rev. Lett. **81**, 4516 (1998).
7. D. Mauri, H. C. Siegmann, P. S. Bagus, and E. Kay, J. Appl. Phys. **62**, 3047 (1987).
8. A. P. Malozemoff, Phys. Rev. B **35**, 3679 (1987).
9. T. Hauet, J. A. Borchers, Ph. Mangin, Y. Henry, and S. Mangin, Phys. Rev. Lett. **96**, 067207 (2006).
10. Steven Brems, Kristiaan Temst, and Chris Van Haesendonck, Phys. Rev. Lett. **99**, 067201 (2007).
11. S. K. Mishra, F. Radu, H. A. Dürr, and W. Eberhardt, Phys. Rev. Lett. **102**, 177208 (2009).
12. S. Maat, K. Takano, S. S. Parkin, and Eric E. Fullerton, Phys. Rev. Lett. **87**, 087202 (2001).
13. J. Olamit, Z. P. Li, I. K. Schuller, and K. Liu, Phys. Rev. B **73**, 024413 (2006).
14. H. Ouyang, K.-W. Lin, C.-C. Liu, Shen-Chuan Lo, Y.-M. Tzeng, Z.-Y. Guo, and J. van Lierop, Phys. Rev. Lett. **98**, 097204 (2007)
15. X. P. Qiu, D. Z. Yang, S. M. Zhou, R. Chantrell, K. O'Grady, U. Nowak, J. Du, X. J. Bai, and L. Sun, Phys. Rev. Lett. **101**, 147207 (2008).
16. K. Liu, S.M. Baker, M. Tuominen, T. P. Russell, I. K. Schuller, Phys. Rev. B **63**, 060403 (2001).
17. J. Sort, A. Hoffmann, S.-H. Chung, K. S. Buchanan, M. Grimsditch, M. D. Baró, B. Dieny, and J. Nogués, Phys. Rev. Lett. **95**, 067201 (2005).
18. J. Stöhr, A. Scholl, T. J. Regan, S. Anders, J. Lüning, M. R. Scheinfein, H. A. Padmore, and R. L. White, Phys. Rev. Lett. **83**, 1862 (1999).
19. H. Ohldag, T. J. Regan, J. Stöhr, A. Scholl, F. Nolting, J. Lüning, C. Stamm, S. Anders, and R. L. White, Phys. Rev. Lett. **87**, 247201 (2001).
20. H. Ohldag, A. Scholl, F. Nolting, E. Arenholz, S. Maat, A. T. Young, M. Carey, and J. Stöhr, Phys. Rev. Lett. **91**, 017203 (2003).

21. S. Roy, M. R. Fitzsimmons, S. Park, M. Dorn, O. Petracic, Igor V. Roshchin, Zhi-Pan Li, X. Batlle, R. Morales, A. Misra, X. Zhang, K. Chesnel, J. B. Kortright, S. K. Sinha, and Ivan K. Schuller, Phys. Rev. Lett. 95, 047201 (2005).

22. Hendrik Ohldag, Hongtao Shi, Elke Arenholz, Joachim Stöhr, and David Lederman, Phys. Rev. Lett. **96**, 027203 (2006).

23. Florin Radu, Alexei Nefedov, Johannes Grabis, Gregor Nowak, Andre Bergmann, Hartmut Zabel, J. Magn. Magn. Mater. **300**, 206 (2006).

24. Sebastian Brück, Gisela Schütz, Eberhard Goering, Xiaosong Ji, and Kannan M. Krishnan, Phys. Rev. Lett. **101**, 126402 (2008).

25. P. Miltényi, M. Gierlings, J. Keller, B. Beschoten, G. Güntherodt, U. Nowak, and K. D. Usadel, Phys. Rev. Lett. **84**, 4224 (2000).

26. Jung-Il Hong, Titus Leo, David J. Smith, and Ami E. Berkowitz, Phys. Rev. Lett. **96**, 117204 (2006).

27. Marian Fecioru-Morariu, Syed Rizwan Ali, Cristian Papusoi, Martin Sperlich, and Gernot Güntherodt, Phys. Rev. Lett. **99**, 097206 (2007).

28. U. Nowak, K. D. Usadel, J. Keller, P. Miltényi, B. Beschoten, and G. Güntherodt, Phys. Rev. B **66**, 014430 (2002).

29. R. Morales, Zhi-Pan Li, J. Olamit, Kai Liu, J. M. Alameda, and Ivan K. Schuller, Phys. Rev. Lett. **102**, 097201 (2009).

30. A. Scholl, M. Liberati, E. Arenholz, H. Ohldag, and J. Stöhr, Phys. Rev. Lett. **92**, 247201 (2004).

31. A. Brambilla, P. Sessi, M. Cantoni, L. Duò, M. Finazzi and F. Ciccacci, Thin Solid Films **516**, 7519 (2008).

32. Gerrit van der Laan, Elke Arenholz, Rajesh V. Chopdekar and Yuri Suzuki, Phys. Rev. **B 77**, 064407 (2008).

33. Elke Arenholz, Gerrit van der Laan,, Rajesh V. Chopdekar, and Yuri Suzuki, Phys. Rev. Lett. **98**, 197201 (2007).

34. I. P. Krug, F. U. Hillebrecht, M. W. Haverkort, A. Tanaka, L. H. Tjeng, H. Gomonay, A. Fraile-Rodríguez, F. Nolting, S. Cramm, and C. M. Schneider, Phys. Rev. B **78**, 064427 (2008).

35. R. Abrudan, J. Miguel, M. Bernien, C. Tieg, M. Piantek, J. Kirschner, and W. Kuch, Phys. Rev. B **77**, 014411 (2008).

36. Jeffrey McCord, Roland Mattheis, and Dieter Elefant, Phys. Rev. B **70**, 094420 (2004).

37. Susumu Soeya, Shigeru Tadokoro, Takao Imagawa, Moriaki Fuyama, and Shinji Narishige, J. Appl. Phys. **74**, 6297 (1993).

38. T.J. Regan, H. Ohldag, C. Stamm, F. Nolting, J. Luning, J. Stohr and R.L. White, Phys.

Rev. B **64**, 214422 (2001).
39. C. Tusche, H.L. Meyerheim, N. Jedrecy, G. Renaud, A. Ernst, J. Henk, P. Bruno, and J. Kirschner, Phys. Rev. Lett. **95**, 176101 (2005).
40. R. Abrudan, J. Miguel, M. Bernien, C. Tieg, M. Piantek, J. Kirschner, and W. Kuch, Phys. Rev. B **77**, 014411 (2008).
41. J. Gurgul *et. al.*, Surf. Interface Anal. (2010). (online preprint, published online 29 Mar 2010.)